Regioselective Hydroformylation of Butadiene: Density Functional Studies†

Chun-Fang Huo,‡ Yong-Wang Li,‡ Matthias Beller,§ and Haijun Jiao*,‡,§

State Key Laboratory of Coal Conversion, Institute of Coal Chemistry, Chinese Academy of Sciences, Taiyuan 030001, People's Republic of China, and Leibniz-Institut für Organische Katalyse an der Universität Rostock e.V., Albert-Einstein-Strasse 29a, 18059 Rostock, Germany

Received January 20, 2005

The $HCo(CO)_3$-catalyzed hydroformylation of butadiene has been investigated at the B3LYP density functional level of theory. It is found that butadiene hydroformylation favors the formal 1,4-addition product in high regioselectivity. The enhanced stability of the *syn*-η^3-allyl complex ($(\eta^3\text{-}CH_2CHCH(CH_3))Co(CO)_3$) presents a distinctly thermodynamic preference for the Markovnikov insertion, and the following CO addition favors forming the 1,4-addition intermediate over the branched intermediate both kinetically and thermodynamically. Neither linear nor branched 1,2-addition product is favored. These results agree perfectly with the experimental findings. Furthermore, it is shown that methanol as solvent does not change the mechanistic picture significantly.

Introduction

As an atom-efficient green route for producing β,γ-unsaturated aldehyde and adipaldehyde (rising from the 1,4-addition and 1,2-addition, respectively), the hydroformylation of butadiene has greatly attracted industrial interest. The optically active β,γ-unsaturated aldehydes are useful chiral building blocks for the stereocontrolled syntheses of natural products.[1−4] Adipaldehyde would be a valuable intermediate for producing ϵ-caprolactam and adipic acid/hexamethylene-1,6-diamine (HMDA), which are key monomers in nylon-6 and nylon-6,6 manufacture.[5−8] Currently, HMDA is mainly obtained from butadiene via hydrocyanide addition or electrochemical coupling reaction with acrylonitrile, followed by adiponitrile hydrogenation.[9,10] Therefore, developing new routes to use economically and easily available raw materials is a significant goal. The hydroformylation of butadiene for obtaining the intermediate, adipaldehyde, is an economical and environmentally friendly method. Although the hydroformylation of olefins is well-studied[11−17] and has had industrial uses on a large scale for many decades, the analogous reaction of butadiene has received less academic attention until now.

As early as 1952, it was recognized that the hydroformylation of butadiene may lead to interesting products such as adipic aldehyde or pentenals.[18] A two-step process using a rhodium and a cobalt catalyst was reported to yield adipic aldehyde (respectively alcohol) with approximately 60% selectivity by BASF.[19] In addition, the systematic studies on the Rh-catalyzed hydroformylation of butadiene were performed by Fell and co-workers.[20−22] It was found that the steric and electronic factors of the phosphine ligands influence the product distribution. Depending on the catalysts employed, various amounts of saturated monoaldehydes and dialdehydes are formed. Secondary phosphines lead to an almost complete 1,4-addition product in the primary step of the hydroformylation of butadiene. In 1985, van Leeuwen and Roobeek[23] successfully hydroformylated butadiene by a 1,2-bis(diphenylphosphino)-ethane-Rh(I) complex to give pentanal in over 90%

† Dedicated to our colleague Professor Dr. Uwe Rosenthal on the occasion of his 55th birthday.

* To whom correspondence should be addressed. E-mail: haijun.jiao@ifok-rostock.de.

‡ State Key Laboratory of Coal Conversion.

§ Leibniz-Institut für Organische Katalyse an der Universität Rostock.

(1) Heathcock, C. H.; Young, S. D.; Hagen, J. P.; Pilli, R.; Badertscher, U. *J. Org. Chem.* **1985**, *50*, 2095.
(2) Evans, D. A.; Di Mare, M. *J. Am. Chem. Soc.* **1986**, *108*, 2476.
(3) Salamonczyk, G. M.; Han, K.; Guo, Z.; Sih, C. J. *J. Org. Chem.* **1996**, *61*, 6893.
(4) Horiuchi, T.; Ohta, T.; Nozaki, K.; Takaya, H. *Chem. Commun.* **1996**, 155.
(5) van Leeuwen, P. W. N. M.; Claver, C. *Rhodium Catalyzed Hydroformylation*; Kluwer Academic Publishers: Dordrecht, The Netherlands, 2000.
(6) Weissermel, K.; Arpe, H.-J. *Industrial Organic Chemistry*, 2nd ed.; VCH: Weinheim, 1993.
(7) Dahlhoff, G.; Niederer, J. P. M.; Hoelderich, W. E. *Catal. Rev.* **2001**, *43*, 381.
(8) Ohgomori, Y.; Suzuki, N.; Sumitani, N. *J. Mol. Catal. A* **1998**, *133*, 289.
(9) Shook, H. E., Jr. U.S. Patent 4,082,811, 1978; *Chem. Abstr.* **1978**, *89*, 109, 935.
(10) King, C. M.; Seidel, W. C.; Tolman, C. A. U.S. Pat. 3,925,445, 1975; *Chem. Abstr.* **1976**, *84*, 88, 921.
(11) (a) Falbe, J. *New Sytheses with Carbon Monoxide*; Springer-Verlag: Berlin, 1980. (b) Torrent, M.; Solà, M.; Frenking, G. *Chem. Rev.* **2000**, *100*, 439.
(12) Beller, M.; Cornils, B.; Frohning, C. D.; Kohlpaintner, C. W. *J. Mol. Catal. A* **1995**, *104*, 17.
(13) Parshall, G. W.; Ittel, S. D. *Homogeneous Catalysis*; Wiley-Interscience: New York, 1992.
(14) Cornils, B.; Herrmann, W. A. *Applied Homogeneous Catalysis with Organometallic Compounds*; Wiley-VCH: Weinheim, 2002; Vol. 1.
(15) Orchin, M.; Rupilius, W. *Catal. Rev.* **1972**, *6*, 85.
(16) Süss-Fink, G.; Meister, G. *Adv. Organomet. Chem.* **1993**, *35*, 41.
(17) Papadogianakis, G.; Sheldon, R. A. *New J. Chem.* **1996**, *20*, 175.
(18) Adkins, H.; Williams, J. R. *J. Org. Chem.* **1952**, *17*, 980.
(19) Kummer, R. (BASF) Ger. Pat. (OLS) 24,14,253, 1974.
(20) Fell, B.; Rupilius, W. *Tetrahedron Lett.* **1969**, *10*, 2721.
(21) Fell, B.; Bahrmann, H. *J. Mol. Catal.* **1977**, *2*, 211.
(22) Bahrmann, H.; Fell, B. *J. Mol. Catal.* **1980**, *8*, 329.
(23) van Leeuwen, P. W. N. M.; Roobeek, C. F. *J. Mol. Catal.* **1985**, *31*, 345.

10.1021/om0500422 CCC: $30.25
Publication on Web 06/18/2005

selectivity. It was suggested that the β,γ-unsaturated aldehyde is formed as the initial product,[24,25] which can further isomerize to the thermodynamically more stable α,β-unsaturated aldehyde.[20] Since the intermediate α,β-unsaturated aldehyde undergoes hydrogenation more readily than hydroformylation,[20,26] the saturated aldehyde is formed. In 1995, Bertozzi et al.[27] reported that the hydroformylation of butadiene promoted by rhodium-mesitylene co-condensate has unusual high chemoselectivity and regioselectivity in the β,γ-unsaturated aldehyde (96%). In 1997, Horiuchi et al.[28] presented a highly selective asymmetric hydroformylation catalyzed by a (*R*,*S*)-BINAPHOS-Rh(I) complex under mild conditions to give an optically active β,γ-unsaturated aldehyde (up to 95%). On the other hand, some attempts at preparing adipaldehyde by butadiene hydroformylation have been made, mainly in the patent literature.[29] In most cases, the selectivity to the desired adipaldehyde is low. Recently, Ohgomori et al.[8] developed a catalyst composed of rhodium and DIOP, with a higher selectivity, about 37%, for the formation of adipaldehyde. Furthermore, they deduced that the ratio of 1,2-addition to 1,4-addition may be determined by the equilibrium of {η^4-(EE)-butadiene}{(AE)-diphospine}(H)Rh and {η^4-(AE)-butadiene}{(EE)-diphospine}(H)Rh.

Regarding the mechanistic aspects, very little basic work has been done. Using online high-pressure IR techniques, Mirbach[30] explored the cobalt-carbonyl-catalyzed hydroformylation of butadiene. The formation of the intermediates, η^3-$C_4H_7Co(CO)_3$ and σ-$C_4H_7Co(CO)_4$, was observed. In the recent IR and NMR study on the pyridine-modified cobalt-catalyzed hydromethoxycarbonylation of butadiene,[31] the existence of the above intermediates was verified, and $C_4H_7Co(CO)_4$ was further characterized as having the 1,4-addition structure $(H_3CHC{=}CHCH_2)Co(CO)_4$. In addition, the deuterioformylation experiment[27] also suggested that the η^3-butenyl complexes are likely to be the key intermediates. As an elementary step in much homogeneous catalysis, the butadiene insertion into the Sm−H bond[32] or Ni−phenyl bond[33] was investigated at the DFT level.

In this paper, a detailed DFT study on the $HCo(CO)_3$-catalyzed hydroformylation of butadiene is performed. A complete mechanistic picture is presented, and the regioselectivity is emphasized and clarified. In addition, the solvent effects of methanol are discussed.

Computational Details

All calculations were performed at the B3LYP/6-311+G(d) density functional level of theory with the Gaussian 03 program.[34] This method is found to be appropriate for cobalt carbonyl chemistry, as indicated by the excellent agreement in vibrational frequencies and bond dissociation energies between theory and experiment.[35] The geometries of each species involved in the catalytic cycle were fully optimized without any symmetry constraints. Furthermore, the frequency analyses were carried out at the same level to confirm the optimized structures to be ground states without imaginary frequency (NImag = 0) or transition states (TS) with one imaginary frequency (NImag = 1). Especially, the single imaginary frequency of each transition state displayed the desired displacement orientation. In addition, the enthalpies and the Gibbs free energies[36] were calculated at actual reaction conditions of 403.15 K and 200 atm in the usual rigid rotor approximation. Considering the entropy effects, the following discussions are based on the free energies (ΔG) of activation and reaction, and the corresponding enthalpies (ΔH) are given in the Supporting Information. For evaluating the solvent effects, the self-consistent reaction field (SCRF) single-point energy calculations on the gas-phase-optimized structures in methanol continuum (methanol as solvent) were carried out by using the isodensity surface polarized continuum model (IPCM)[37] at the B3LYP/6-311+G(d) level. The solvation free energy is the free energy difference between solution and gas phase. Furthermore, the calculated total electronic energies, ZPE, and thermal corrections to enthalpies and Gibbs free energies are provided in the Supporting Information.

Results and Discussion

Since butadiene can be considered a substituted olefin, one can conceive that the mechanism of butadiene hydroformylation is similar to olefins[38] to some extent. However, butadiene hydroformylation has some special characteristics due to the presence of an additional conjugated vinyl group. Based on the Heck−Breslow mechanism[39] and on the high-pressure IR results of the reactions of conjugated dienes with cobalt carbonyls under hydroformylation conditions,[30] three possible pathways of butadiene hydroformylation for producing unsaturated monoaldehydes are proposed and shown in Scheme 1. Path 1 is the *anti*-Markovnikov reaction with the formation of linear aldehyde in 1,2-addition fashion (**AM**), and paths 2 and 3 are the Markovnikov reaction with the formation of linear aldehyde in 1,4-addition fashion (**ML**) and branched aldehyde in 1,2-addition fashion (**MB**), respectively. Following these reaction paths, the $HCo(CO)_3$-catalyzed butadiene hydroformylation is thoroughly investigated. The elementary steps, butadiene insertion and CO addition, are emphasized to elucidate the origin of the regioselectivity, while other steps are briefly discussed. After that, the solvent effects are addressed.

(1) Butadiene Coordination. It is well known that butadiene exists in two minimum energy conformers, *trans* and *cis*, and the former is more stable by 3.5 kcal/mol. Therefore, the following discussion mainly focuses on the coordination modes of *trans*-butadiene. Rising from the conjugated structure, butadiene can coordinate to the cobalt carbonyl moiety in either mono-

(24) Brown, C. K.; Mowat, W.; Yagupsky, G.; Wilkinson, G. *J. Chem. Soc. A* **1971**, 850.
(25) Botteghi, C.; Branca, M.; Saba, A. *J. Organomet. Chem.* **1980**, *184*, C17.
(26) Botteghi, C.; Salomon, C. *Tetrahedron Lett.* **1974**, *15*, 4285.
(27) Bertozzi, S.; Campigli, N.; Vitulli, G.; Lazzaroni, R.; Salvadori, P. *J. Organomet. Chem.* **1995**, *487*, 41.
(28) Horiuchi, T.; Ohta, T.; Shirakawa, E.; Nozaki, K.; Takaya, H. *Tetrahedron* **1997**, *53*, 7795.
(29) (a) Kummer, R.; Weiss, F. J. *Symp. Rhodium Homogeneous Catal.* **1978**, 87. (b) Packett, D. L. Eur. Pat. Appl. EP 577,042, 1993; *Chem. Abstr.* **1994**, *120*, 298075j. (c) Packett, D. L. U.S. Pat. 5,312,996, 1994; *Chem. Abstr.* **1995**, *123*, 82828w.
(30) Mirbach, M. F. *Transition Metal Chem.* **1984**, *9*, 465.
(31) Tuba, R.; Mika, L. T.; Bodor, A.; Pusztai, Z.; Tüth, I.; Horváth, I. T. *Organometallics* **2003**, *22*, 1582.
(32) Kaita, S.; Koga, N.; Hou, Z.; Doi, Y.; Wakatsuki, Y. *Organometallics* **2003**, *22*, 3077.
(33) Tobisch, S.; Taube, R. *J. Organomet. Chem.* **2003**, *683*, 181.
(34) Frisch, M. J.; et al. *Gaussian 03*; Gaussian, Inc.: Pittsburgh, PA, 2003.
(35) Huo, C.-F.; Li, Y.-W.; Wu, G.-S.; Beller, M.; Jiao, H. *J. Phys. Chem. A* **2002**, *106*, 12161.
(36) Ochterski, J. W. *Thermochemistry in Guassian* (see: help@Gaussian.com).
(37) Foresman, J. B.; Keith, T. A.; Wiberg, K. B.; Snoonian, J.; Frisch, M. J. *J. Phys. Chem*. **1996**, *100*, 16098.
(38) Huo, C.-F.; Li, Y.-W.; Beller, M.; Jiao, H. *Organometallics* **2003**, *22*, 4665.
(39) Heck, R. F.; Breslow, D. S. *J. Am. Chem. Soc.* **1961**, *83*, 4023.

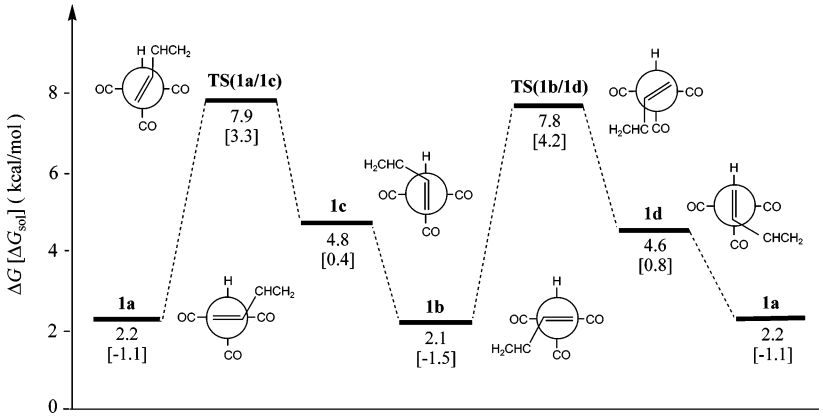

Figure 1. Free energy profile (kcal/mol, in gas phase and in solution) with the Newman projection for η^2-butadiene coordination (relative to $HCo(CO)_3$ + butadiene in gas phase).

Scheme 1. Proposed Mechanism of Butadiene Hydroformylation for Producing Unsaturated Monoaldehydes

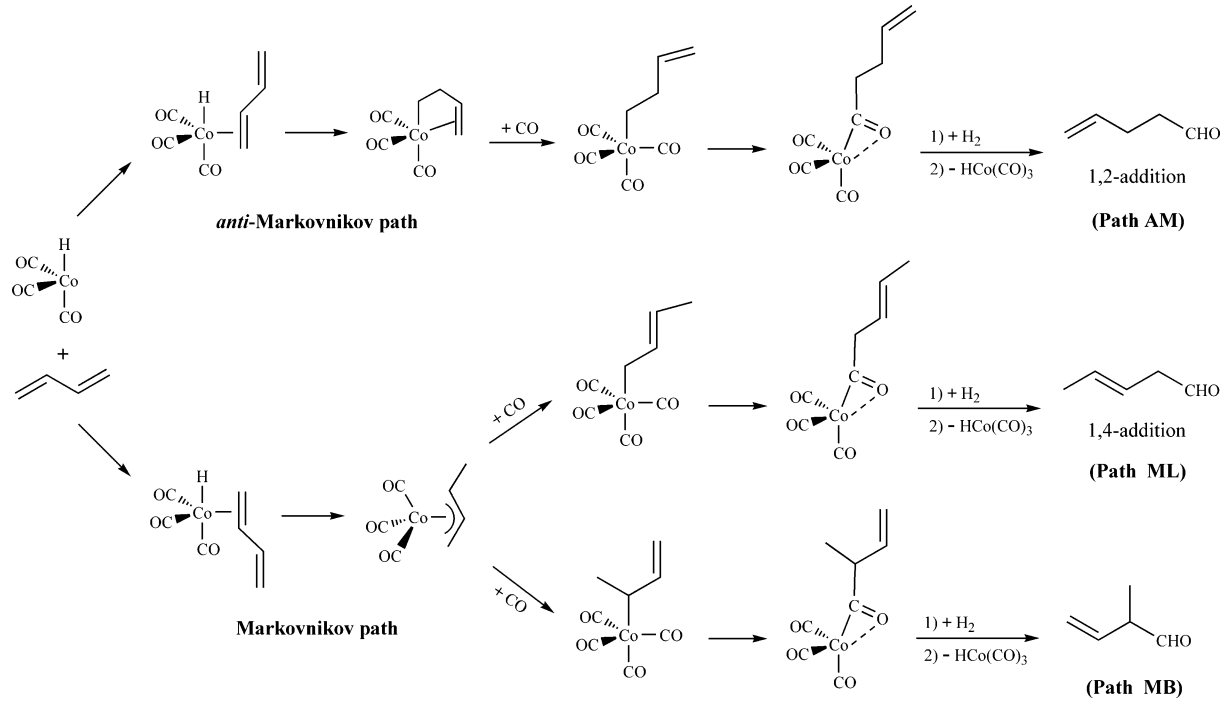

dentate or bidentate fashion. For the unmodified Co-based catalytic system, the active catalyst species is the planar C_{2v} $HCo(CO)_3$.[35] This 16-electron species is then trapped by butadiene via the monodentate mode, leading to the π complex $HCo(CO)_3(\eta^2\text{-}CH_2{=}CHCH{=}CH_2)$. For this η^2-*trans* coordination mode, the potential energy surface of $HCo(CO)_3(\eta^2\text{-}CH_2{=}CHCH{=}CH_2)$ is similar to that of propene,[38] as shown in Figure 1. The corresponding structures are given in the Supporting Information.

Trans-Butadiene coordination to $HCo(CO)_3$ forms the most stable π complex, $HCo(CO)_3(\eta^2\text{-}CH_2{=}CHCH{=}CH_2)$ (**1a** and **1b**), with the coordinated C=C bond in the equatorial plane. This process is predicted to be endergonic by 2.2 and 2.1 kcal/mol, while exothermic by 11.4 and 11.5 kcal/mol, respectively. Furthermore, the low rotation barriers of 2.4−5.7 kcal/mol indicate that **1a** and **1b** can facilely convert to **1c** and **1d**, in which the coordinated C=C bond is parallel to the Co−H bond. This transformation facilitates the subsequent insertion of η^2-$CH_2{=}CHCH{=}CH_2$ into the Co−H bond.

To obtain further insight into the potential energy surface of the η^2-butadiene complex, the most stable conformer of η^2-*cis*-butadiene coordination has also been located. As expected, the energy gap between *trans* and *cis* forms of free butadiene is preserved in the related complexes. It is found that the η^2-*trans*-butadiene complex is still energetically preferred by 2.8 kcal/mol. Taking the solvent effect into account, the energy difference increases to 3.5 kcal/mol. Therefore, the η^2-*trans*-butadiene complex should be more dominant over the η^2-*cis*-butadiene complex. This case is analogous to the recent DFT results of $Cp^*_2SmH(\eta^2\text{-butadiene})$ ($Cp^* = \eta^5\text{-}C_5Me_5$)[32] and $Ni^{II}(\eta^5\text{-Cp})(\eta^1\text{-phenyl})(\eta^2\text{-butadiene})$.[33] Apart from the η^2-coordination mode, we also are interested in the η^4-coordination of butadiene. Butadiene coordinates to the $HCo(CO)_2$ moiety via the η^4 mode, leading to two trigonal bipyramid complexes with hydride at the axial site, i.e., butadiene at the diequatorial (ee) or the axial−equatorial (ae) positions. For analyzing the thermodynamic competition of the two modes, one can consider a dissociation/association equilibrium be-

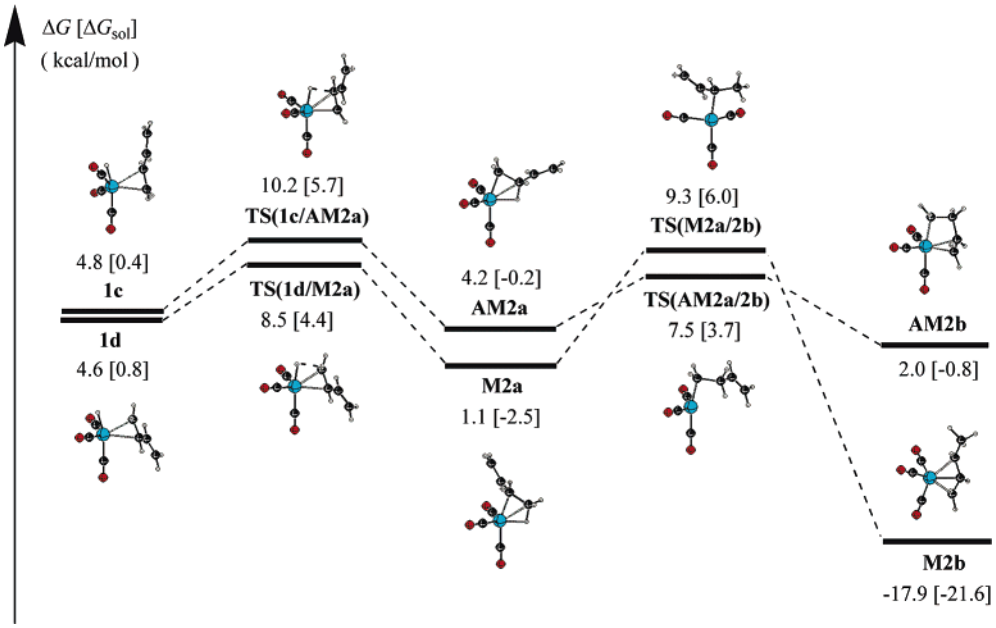

Figure 2. Free energy profiles (kcal/mol, in gas phase and in solution) for butadiene insertion (relative to $HCo(CO)_3$ + butadiene in gas phase).

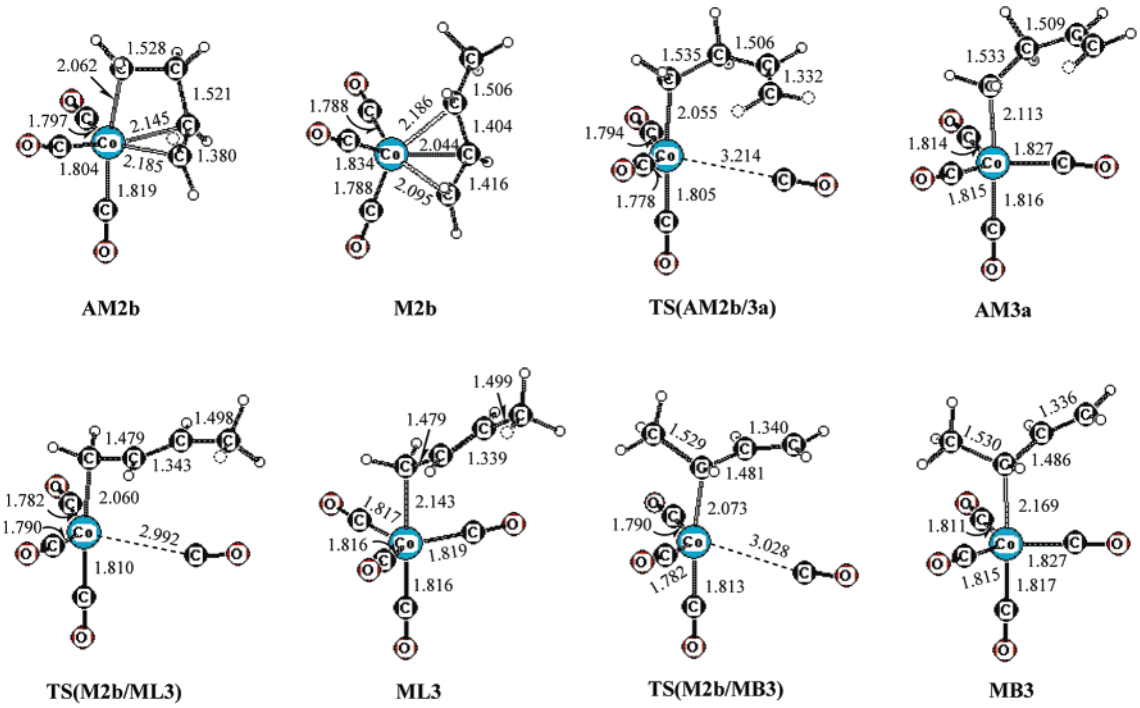

Figure 3. Bond parameters (in Å) of the key stationary points involved in butadiene insertion and CO addition process.

tween $HCo(CO)_3(\eta^2$-butadiene) and $HCo(CO)_2(\eta^4$-butadiene) as in eqs 1 and 2. The large endergonic values of 17.5 and 14.7 kcal/mol indicate that the η^2-*trans* form is more favorable thermodynamically.

$$HCo(CO)_3(\eta^2\text{-}CH_2{=}CHCH{=}CH_2)\ (\mathbf{1a}) = HCo(CO)_2(\eta^4\text{-}CH_2{=}CHCH{=}CH_2/ee) + CO$$
$$\Delta G = 17.5\ \text{kcal/mol} \quad (1)$$

$$HCo(CO)_3(\eta^2\text{-}CH_2{=}CHCH{=}CH_2)\ (\mathbf{1a}) = HCo(CO)_2(\eta^4\text{-}CH_2{=}CHCH{=}CH_2/ae) + CO$$
$$\Delta G = 14.7\ \text{kcal/mol} \quad (2)$$

(2) η^2-Butadiene Insertion. Starting with **1c** and **1d**, η^2-butadiene insertion into the Co−H bond forming butenyl complexes can take place in *anti*-Markovnikov and Markovnikov ways, respectively. The free energy profile for this process is reported in Figure 2, and the structures of stationary points are given in the Supporting Information. Some key structures are shown in Figure 3.

As shown in Figure 2, the η^2-butadiene insertion reaction proceeds in steps. First, the hydride transfers to the carbon atoms of the coordinated C=C bond, forming the butenyl group. This step goes via the trigonal bipyramidal transition states, **TS(1c/AM2a)** and **TS(1d/M2a)**, leading to the Co···H−C agostic

stabilized intermediates **AM2a** and **M2a**, respectively. The free energy profiles in Figure 2 clearly show that the hydride migration processes (**1c → TS(1c/AM2a) → AM2a** and **1d → TS(1d/M2a) → M2a**) are slightly exergonic by 0.6 and 3.5 kcal/mol and need to overcome the low free energy barriers of 5.4 and 3.9 kcal/mol. A similar case has been found for propene.[38] However, it is noteworthy that the substituent of the vinyl group has imposed an influence on the relative stability of the *anti*-Markovnikov and Markovnikov species. The *anti*-Markovnikov species **TS(1c/AM2a)** and **AM2a** are predicted to be higher in free energy than the corresponding Markovnikov species **TS(1d/M2a)** and **M2a** by 1.7 and 3.1 kcal/mol. Therefore, the formation of **M2a** is more favored both kinetically and thermodynamically.

The following step is the further isomerization of **AM2a** or **M2a** to form the more stable conformation **AM2b** or **M2b**, in which the C=C bond participates in the coordination to $Co(CO)_3$. As shown in Figure 3, the *anti*-Markovnikov intermediate **AM2b** has a trigonal bipyramidal geometry with the butenyl group at the axial−equatorial site. In **AM2b**, the butenyl group coordinates to the $Co(CO)_3$ moiety in η^3 mode, forming a structure that consists of a four-membered ring and a three-membered ring. In addition, we have considered the possibility of forming the six-membered ring through a Co···H−C (H_2C=) agostic interaction. Taking this conformation as the starting point, the optimization leads to **AM2b** directly. Unlike the *anti*-Markovnikov intermediate **AM2b**, the Markovnikov intermediate **M2b** has a square pyramidal geometry with a η^3-coordination of the allylic $CH_2CHCHCH_3$ group to $Co(CO)_3$. Furthermore, two corresponding transition states for the rotation of the butenyl group, **TS(AM2a/2b)** and **TS(M2a/2b)**, have been located. Both transition states have butterfly geometries with the η^1-coordinated butenyl group at the axial site. From the free energy profiles in Figure 2, we can find that the agostic *anti*-Markovnikov intermediate **AM2a** and the η^3-butenyl complex **AM2b** are in a fast equilibrium, indicated by the low free energy barrier of 3.3 kcal/mol and the slightly exergonic property. In contrast, the transformation of the agostic Markovnikov intermediate **M2a** to the *syn*-η^3-allyl complex **M2b** is a highly exergonic (−19.0 kcal/mol) and irreversible process, while it has a moderate free energy barrier of 8.2 kcal/mol.

On the basis of the above discussions, we will address the competition of the *anti*-Markovnikov and Markovnikov insertion of η^2-*trans*-butadiene. The probability of the alternative insertion pathways is entirely discriminated by the respective total barrier and the relative stability of the insertion products. Summarizing the data in Figures 1 and 2, we can map out the completed energy surface for the butadiene insertion. It is distinct that the *anti*-Markovnikov (**1b** to **AM2b**) and Markovnikov (**1a** to **M2b**) insertion have different thermodynamic behavior. The *anti*-Markovnikov insertion (**1b** to **AM2b**) is predicted to be a thermally neutral (−0.1 kcal/mol) and reversible process and can be accomplished by overcoming a total free energy barrier of 8.1 kcal/mol. However, the Markovnikov insertion (**1a** to **M2b**) is a highly exergonic (−20.1 kcal/mol) and irreversible process, with an insertion free energy barrier of 6.3 kcal/mol. The difference of 1.8 kcal/mol for the insertion energy barriers indicates that the Markovnikov insertion should be kinetically more favored than the *anti*-Markovnikov insertion. Furthermore, the Markovnikov insertion product **M2b** is thermodynamically more stable than the *anti*-Markovnikov insertion product **AM2b** by 19.9 kcal/mol. This indicates that the Markovnikov insertion is the only favored path leading to the *syn*-η^3-allyl complex **M2b** as the principal intermediate, in agreement with the IR and NMR results.[30,31] In addition, it is found that the *anti*-isomer of the allylic complex **M2b** is higher in free energy than the *syn*-isomer by 2.5 kcal/mol (3.2 kcal/mol in solvent). The *syn/anti* isomerization of the allylic complex (**M2b**) is computed to be a $\eta^3 \rightarrow \eta^1 \rightarrow \eta^3$ transformation process, as shown in the Supporting Information. The corresponding transition state **TS(M2b/M2b′)** is a η^1-species having an agostic interaction between the central C−H bond of the allyl group and the cobalt atom, similar to the case of the allylpalladium complexes reported by Solin et al.[40] Due to the break of two Co−C bonds, this isomerization process has a high free energy barrier of 26.7 kcal/mol (26.9 kcal/mol in solvent), which is higher than that of the insertion process.

For complete comparison, we have also computed the η^2-*cis*-butadiene insertion reaction. The geometries and energies for the corresponding transition states and intermediates are provided in the Supporting Information. As expected, the free energy barriers for η^2-*cis*-butadiene insertion in both *anti*-Markovnikov and Markovnikov paths (7.8 and 5.9 kcal/mol) are very close to those for η^2-*trans*-butadiene insertion (8.1 and 6.3 kcal/mol), respectively. Combining the kinetic and thermodynamic effects discussed above, the butadiene hydroformylation occurs via the η^2-*trans*-butadiene insertion path.

(3) CO Addition and Insertion. Following the butadiene insertion, the CO addition and insertion take place. As shown in Scheme 1, CO addition to the η^3-butenyl complex **AM2b** (*anti*-Markovnikov intermediate) forms the 1,2-addition intermediate $(H_2C{=}CHCH_2CH_2)Co(CO)_4$, while CO addition to the *syn*-η^3-allyl complex **M2b** (Markovnikov intermediate) leads to the 1,4-addition intermediate $(H_3CHC{=}CHCH_2)Co(CO)_4$ and the branched intermediate $(H_2C{=}CHCH(CH_3))Co(CO)_4$, respectively. The energy profiles associated with these processes are depicted in Figure 4, while the structures of several key stationary points involved in CO addition are illustrated in Figure 3, and the others are given in the Supporting Information.

On the basis of the conformation of the η^3-butenyl complex **AM2b**, the incoming CO would enter the cobalt coordination sphere by attacking the C=C bond occupied equatorial site (Figure 4, top). This leads to the trigonal bipyramidal complex **AM3a** ($(H_2C{=}CHCH_2CH_2)Co(CO)_4$), in which the butenyl group stands at the axial site in the η^1-coordination mode. In the corresponding transition state **TS(AM2b/3a)**, the interaction between cobalt and the C=C bond has broken, although the new Co−C bond (3.214 Å) is still very weak (Figure 3). As shown in the top free energy profile of Figure 4, this CO addition process is exergonic by 2.3 kcal/mol and has a moderate free energy barrier of 13.8 kcal/mol. Interestingly, the butenyl tetracarbonyl complex **AM3a**

(40) Solin, N.; Szabó, K. J. *Organometallics* **2001**, *20*, 5464.

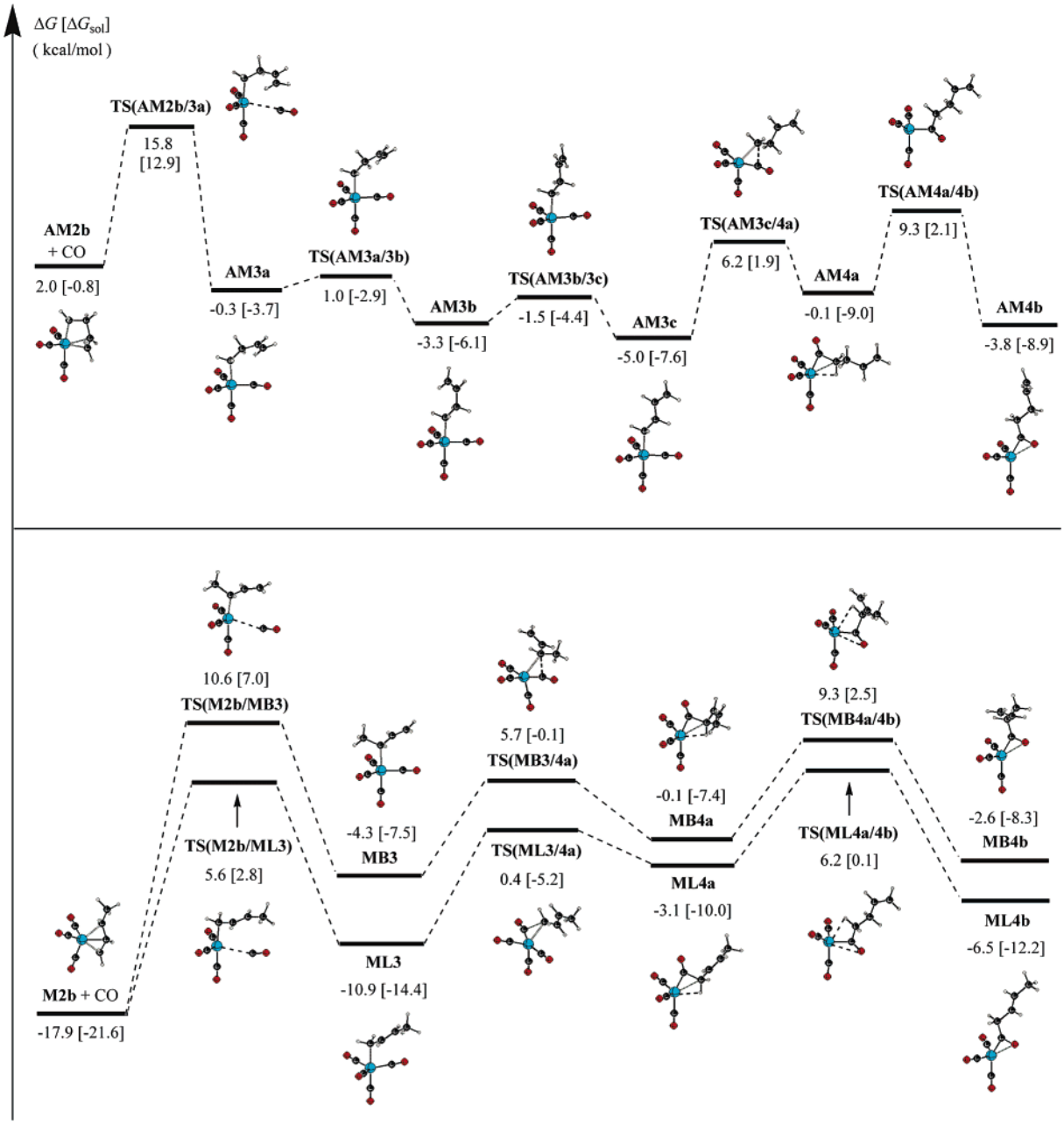

Figure 4. Free energy profiles (kcal/mol, in gas phase and in solution) for CO addition and insertion (top for *anti*-Markovnikov path and bottom for Markovnikov path, relative to $HCo(CO)_3$ + butadiene + CO in gas phase).

can further convert to the more stable isomers **AM3b** and **AM3c** by the rotation of the $CH_2-CH_2CHCH_2$ bond and the $CH_2CH_2-CHCH_2$ bond, respectively. Compared with **AM3a**, **AM3b** and **AM3c** are lower in free energy by 3.0 and 4.7 kcal/mol. The rather small rotation barriers of 1.3 and 1.8 kcal/mol indicate that these transformations can proceed very facilely.

As mentioned above, CO addition to the Markovnikov intermediate, *syn*-η^3-allyl complex **M2b**, is more complicated. According to the conformation of *syn*-η^3-allyl complex **M2b**, the incoming CO can attack **M2b** from the front or the back side of the 1-methyl-allyl group (η^3-$H_2CCHCHCH_3$). Accompanying the CO approach, the η^3-coordination 1-methyl-allyl group should switch to the η^1-coordination mode. During this course, the π electrons can locate in different C−C bonds, forming the $HC{=}CHCH_3$ and $H_2C{=}CH$ bond, respectively. As illustrated in Figure 4 (bottom), CO attack from the Co−$CHCH_3$ side proceeds via the transition state **TS(M2b/ML3)**, leading to the 1,4-addition intermediate **ML3** ($(H_3CHC{=}CHCH_2)Co(CO)_4$) (the attack from back side via **TS′(M2b/ML3)** to **ML3** is very close in energy), while CO attack from the Co−CH_2 side goes via the transition state **TS(M2b/MB3)**, giving the branched intermediate **MB3** ($(H_2C{=}CHCH(CH_3))Co(CO)_4$). In all cases, the transition states and the addition products have the trigonal bipyramidal geometries with the butenyl group at the axial site (Figure 3). The bottom free energy profiles in Figure 4 clearly show that the alternative paths (**M2b** → **TS(M2b/ML3)** → **ML3** and **M2b** → **TS(M2b/MB3)** → **MB3**) are endergonic by 7.0 and 13.6 kcal/mol and can be accomplished by overcoming the high free energy barriers of 23.5 and 28.5 kcal/mol. This thermodynamic behavior strongly differs from that of propene.[38] It was found that CO addition to the $(C_3H_7)Co(CO)_3$ is a highly exergonic and irrevers-

ible process. However, the endergonic behavior and high energy barrier for CO addition in butadiene hydroformylation are supported by experiments. In the related high-pressure IR study,[30] for example, not only was the formation of the π-allyl complex η^3-$C_4H_7Co(CO)_3$ observed, but also the existence of σ-$C_4H_7Co(CO)_4$ was confirmed. In addition, they attributed the slow hydroformylation rates to the catalytic inertness of the π-allyl complex η^3-$C_4H_7Co(CO)_3$, in line with our theoretical results.

At this stage, analyzing the competition of two CO addition paths (path **ML** and **MB**) is very interesting and necessary. From the bottom free energy profiles in Figure 4, it is evident that the 1,4-addtion species **TS(M2b/ML3)** and **ML3** are lower in free energy than the corresponding branched species **TS(M2b/MB3)** and **MB3** by 5.0 and 6.6 kcal/mol. Therefore, the formation of **ML3** is more favored both kinetically and thermodynamically. Furthermore, what is the driving force for these energy differences? Comparing the bond parameters of the corresponding species in Figure 3, we can find that the Co−$C_{butenyl}$ distances (2.060 and 2.143 Å) in **TS(M2b/ML3)** and **ML3** are shorter than those (2.073 and 2.169 Å) in **TS(M2b/MB3)** and **MB3**, respectively. This indicates that a stronger steric interaction exists between the isobutenyl group and the $Co(CO)_4$ unit, and thus **TS(M2b/MB3)** and **MB3** are less favored energetically than **TS(M2b/ML3)** and **ML3**. This is in line with the relative stability of propyl and isopropyl cobalt tetracarbonyl complexes.[38] The above results suggest that the CO addition process is another crucial factor for determining the observed regioselectivity.

The subsequent CO insertion step proceeds along three pathways, **AM3c** → **AM4a** → **AM4b** (path **AM**), **ML3** → **ML4a** → **ML4b** (path **ML**), and **MB3** → **MB4a** → **MB4b** (path **MB**), forming the acyl complexes. From the right free energy profiles in Figure 4, we can see that the CO insertion process for butadiene hydroformylation is similar to that for propene.[38] It proceeds via two $Co(CO)_3$ pseudorotated transition states and a Co···H−C agostic stabilized intermediate leading to the η^2-O=C stabilized acyl complex. The whole insertion process is predicted to be endergonic by 1.2, 4.4, and 1.7 kcal/mol, with the total free energy barriers of 14.3, 17.1, and 13.6 kcal/mol for path **AM**, **ML**, and **MB**, respectively. It is noteworthy that the transition states and intermediates of path **ML** are more stable than the corresponding species of path **MB**.

(4) H_2 Oxidative Addition and Unsaturated Aldehyde Reductive Elimination. The following steps of the catalytic cycle are to produce the unsaturated aldehydes as initial products. As expected, the H_2 oxidative addition and aldehyde reductive elimination processes for butadiene hydroformylation are similar to those for propene.[38] Therefore, we only discuss the energetic changes based on the free energy profiles in Figure 5, while the structural parameters are given in the Supporting Information.

As depicted in Figure 5 (left), H_2 coordination to the η^2-O=C acyl complex forming the hydrogen complex (**AM4b** → **AM5a**, **ML4b** → **ML5a**, and **MB4b** → **MB5a**) is predicted to be endergonic by 11.8, 11.3, and 12.0 kcal/mol, respectively. The successive H_2 oxidative addition (**AM5a** → **AM5b** → **AM6**, **ML5a** → **ML5b** → **ML6**, and **MB5a** → **MB5b** → **MB6**) proceeds by stepping via the acyl group rotation and the H−H dissociation leading to the dihydride complex, and the entire process is computed to be endergonic by 4.1, 4.3, and 2.6 kcal/mol, with the total free energy barriers of 5.7, 5.9, and 5.9 kcal/mol. The right free energy profiles in Figure 5 clearly show that the unsaturated aldehyde elimination (**AM6** → **AM7**, **ML6** → **ML7**, and **MB6** → **MB7**) is a rapid and irreversible process, which goes through the three-center transition state giving the unsaturated aldehyde adduct. Interestingly, the energetic preference for the species along path **ML** with respect to the corresponding species along path **MB** is still preserved in these processes.

(5) Regioselectivity. The hydroformylation of butadiene can give the 1,2-addition unsaturated aldehyde H_2C=$CHCH_2CH_2CHO$, the 1,4-addition unsaturated aldehyde H_3CHC=$CHCH_2CHO$, and the branched unsaturated aldehyde H_2C=$CHCH(CH_3)CHO$ as initial products (Scheme 1). For the $HCo(CO)_3$-catalyzed hydroformylation of butadiene, the observed regioselectivity is determined by η^2-butadiene insertion into the Co−H bond and CO addition steps.

Combining the results in Figures 1 and 2, we can find that the thermodynamic behavior of the *anti*-Markovnikov insertion and the Markovnikov insertion is remarkably different. The *anti*-Markovnikov insertion (**1b** to **AM2b**) is a reversible process, while the Markovnikov insertion (**1a** to **M2b**) is an irreversible process. Although the difference of the total insertion free energy barriers for both paths is small (8.1 and 6.3 kcal/mol), the rather high stability (19.9 kcal/mol) of the *syn*-η^3-allyl complex **M2b** with respect to **AM2b** presents a distinctively thermodynamic preference for the Markovnikov insertion. This leads to the *syn*-η^3-allyl complex **M2b** as the exclusive intermediate of the butadiene insertion, and thus the formation of 1,2-addition product via the *anti*-Markovnikov intermediate **AM2b** is almost suppressed.

The subsequent CO addition to the Markovnikov intermediate, *syn*-η^3-allyl complex **M2b**, can give **ML3** ($(H_3CHC$=$CHCH_2)Co(CO)_4$) and **MB3** ($(H_2C$=$CHCH(CH_3))Co(CO)_4$). The former eventually leads to the 1,4-addition product (path **ML**), while the latter eventually yields the branched product (path **MB**). As shown in Figure 4 (left of the bottom energy profiles), the 1,4-addition species **TS(M2b/ML3)** and **ML3** are lower in free energy than the corresponding branched species **TS(M2b/MB3)** and **MB3** by 5.0 and 6.6 kcal/mol, respectively. These energy differences favor the 1,4-addition product over the branched product with a percentage ratio of nearly 100% both kinetically and thermodynamically.

As a consequence, the $HCo(CO)_3$-catalyzed butadiene hydroformylation proceeds along path **ML**, leading to the 1,4-addition unsaturated aldehyde H_3CHC=$CHCH_2CHO$ as the initial principal product, in line with the experimental observations. The free energy data of each elementary step involved in this favored path are collected in Table 1. It is clearly shown that *syn*-η^3-allyl complex **M2b** is the resting state of the catalyst. The CO addition has the largest free energy barrier and should be the rate-determining step.

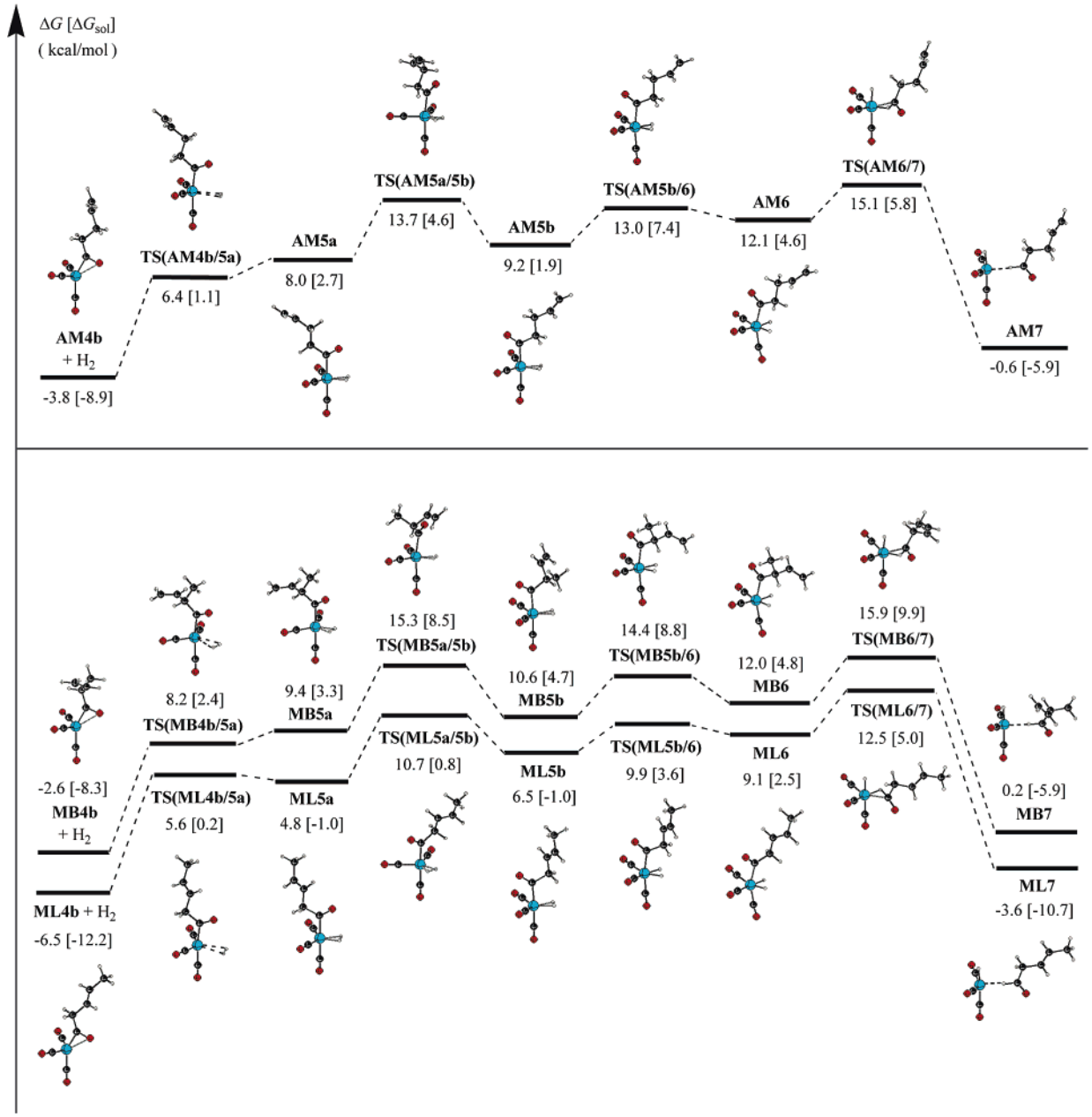

Figure 5. Free energy profiles (kcal/mol, in gas phase and in solution) for H_2 oxidative addition and aldehyde elimination (top for *anti*-Markovnikov path and bottom for Markovnikov path, relative to $HCo(CO)_3$ + butadiene + CO + H_2 in gas phase).

(6) Comparison with Experiment. Recently, several key intermediates of cobalt-catalyzed hydromethoxycarbonylation of butadiene have been characterized by using high-pressure IR and NMR techniques.[31] Four facts are found for the catalytic cycle and the reaction mechanism: (i) the allylic complex (η^3-C_4H_7)$Co(CO)_3$ (**M2b**) is quite stable at 100 °C, and no further reactions could be detected after the formation for several hours under 75 bar of CO at 100 °C in MeOH; (ii) but-2-enyl complex ($CH_3CH{=}CHCH_2$)$Co(CO)_4$ (**ML3**) is very unstable and can be readily converted to the corresponding acyl complex ($CH_3CH{=}CHCH_2CO$)$Co(CO)_4$ with CO (quantitative formation at −40 °C under 70 bar of CO); (iii) **ML3** can be very easily converted to **M2b** by losing CO by raising the reaction temperature from −40 °C to room temperature; (iv) the acyl complex ($CH_3CH{=}CHCH_2CO$)$Co(CO)_4$ is stable at 0 °C under 70 bar of CO, but can be easily converted to **M2b** at higher temperature (>40 °C) by decarbonylation reaction.

Although there are no quantitative kinetic and thermodynamic data available for direct comparison, these experimental results agree qualitatively with our computations. The changes of free energies and enthalpies (note that these values are scaled at 130 °C) are shown in Scheme 2. For example, **ML3** by losing CO resulting in **M2b** is thermally neutral (1.1 kcal/mol), but the large entropy effect leads to a negative free energy change (−7.0 kcal/mol). This is why **ML3** to **M2b** can be conducted by raising the temperature (−40 °C to room temperature). The same explanation is also found for the formal change from the acyl complex by losing two CO molecules to **M2b** at even higher temperature (140 °C), since this formal process is endothermic (9.3 kcal/mol), but exergonic (−7.9 kcal/mol) due to the large

Table 1. Free Energies of Activation and Reaction ($\Delta G^{\ddagger}$ and ΔG, kcal/mol) for the Most Favored Path, ML

reaction	$\Delta G^{\ddagger}$ [$\Delta G_{sol}^{\ddagger}$][a]	ΔG [ΔG_{sol}][a]
butadiene insertion		
1a → 1d	2.4 [1.9]	2.4 [1.9]
1d → TS(1d/M2a) → M2a	3.9 [3.6]	−3.5 [−3.3]
M2a → TS(M2a/2b) → M2b	8.2 [8.5]	−19.0 [−19.1]
CO addition and insertion		
M2b + CO → TS(M2b/ML3) → ML3	23.5 [24.4]	7.0 [7.5]
ML3 → TS(ML3/4a) → ML4a	11.3 [9.2]	7.8 [4.4]
ML4a → TS(ML4a/4b) → ML4b	9.3 [10.1]	−3.4 [−2.2]
H_2 oxidative addition		
ML4b + H_2 → TS(ML4b/5a) → ML5a	12.1 [12.4]	11.3 [11.2]
ML5a → TS(ML5a/5b) → ML5b	5.9 [1.8]	1.7 [0.0]
ML5b → TS(ML5b/6) → ML6	3.4 [4.6]	2.6 [3.5]
aldehyde elimination		
ML6 → TS(ML6/7) → ML7	3.4 [2.5]	−12.7 [−13.2]

[a] The corresponding data with methanol as solvent are given in square brackets.

Scheme 2. Relative Free Energies (in kcal/mol, enthalpies in square brackets): Relationship among Various Key Intermediates

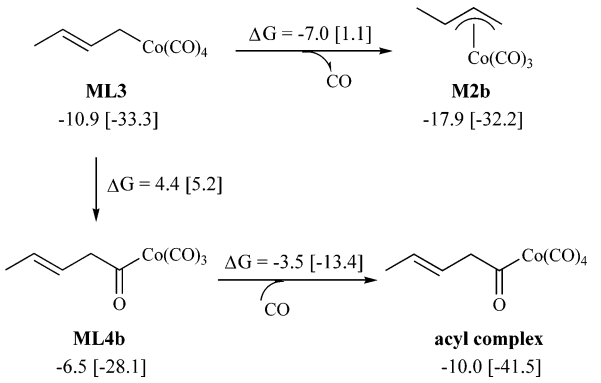

Table 2. Computed[a] and Detected CO Stretching Frequencies (ν_{CO}, cm^{-1})

system	ν_{CO}/calc	ν_{CO}/expt[b]
M2b	1994 (vs), 1996 (vs), 2049 (s)	1988 (vs), 2057 (s) [1993 (vs), 2060 (s)][c]
ML3	2010 (s), 2016 (s), 2028 (m), 2084 (w)	2005 (s), 2011 (s), 2028 (m), 2099 (w)
acyl complex	2004 (s), 2021 (s), 2043 (m), 2094 (w), 1728 (w)	2007 (s), 2026 (s), 2047 (m), 2108 (w), 1710 (w)
ML4b	1983 (s), 2010 (m), 2071 (m), 1690 (w)	[1977, 2008, 2081, 1686][d]

[a] At B3LYP/6-311+G(d), scaled by an empirical factor of 0.9667 deduced from the free CO frequency at the same level. [b] Reference 31. [c] Reference 30. [d] Reference 42 for $(CH_3CO)Co(CO)_3$.

entropy contribution. In addition, the exothermic property (−8.2 kcal/mol) from **ML3** to the acyl complex explains the facial reaction at low temperature (−40 °C).

Furthermore, we have also compared the calculated and detected CO stretching frequencies of these intermediates. As given in Table 2, the calculated values agree perfectly with the experimental data. The linear relationship between the calculated and detected CO frequencies in Scheme 3 is self-explaining on the quality of the calculation and in turn confirms the experimental findings.

(7) Solvent Effects. One of the most frequently asked questions in general is the solvent effects in

Scheme 3. Correlation (R^2 = 0.992) between Calculated and Detected CO Frequencies (ν_{CO}, cm^{-1}) for the Intermediates

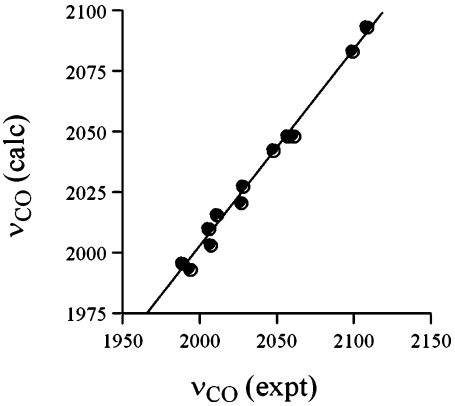

computation, since most of the reactions take place in solvents rather in ideal gas phase. Here we performed a set of calculations to estimate the magnitudes of solvation in hydroformylation of butadiene. In our model calculation, we have used methanol as solvent due to its polarity, forming a continuous medium on one hand, and on the other hand, as reactant for hydromethoxycarbonylation. Comparison between gas phase and medium calculations can provide insight into the effect of solvent on the reaction potential energy surface and the change of reaction mechanism.

First, the dielectric effect of methanol on all species is estimated using the IPCM model. The data are given in square brackets of the corresponding free energy profiles in Figures 1, 2, 4, and 5. These results show that the solvation free energy for the species involved in butadiene coordination (Figure 1), butadiene insertion (Figure 2), and CO addition (Figure 4) is in the range 2.6−4.5 kcal/mol, while the species involved in CO insertion (Figure 4), H_2 oxidative addition, and aldehyde elimination (Figure 5) have a slightly larger solvation free energy of 5.5−7.5 kcal/mol. However, the free energies of activation and reaction in methanol are comparable with the data in the gas phase. Along the reaction path **ML** for forming the 1,4-addition product (Table 1), most changes are within 1.0 kcal/mol, but some significant lowering of energy barriers is found in the CO insertion and H_2 oxidative addition steps, e.g., −2.1 kcal/mol for **ML3 → ML4a** and −4.1 kcal/mol for **ML5a → ML5b**, respectively. However, no disorders of the stationary points on the energy profiles due to solvation can be found.

Since the CO addition step has the highest free energy of activation and negligible solvent effects, these changes in CO insertion and H_2 oxidative addition do not affect the rate-determining step. This indicates that a polar solvent like methanol can stabilize species involved in the catalytic cycle to some extent, but cannot change their relative values in activation and reaction.

In addition, we have also considered the possibility of methanol as ligand for changing the reaction mechanism or alternating the reaction rate. Three competing reactions have been examined: (i) methanol and butadiene with the active catalyst, $HCo(CO)_3$, (ii) methanol and CO with the η^3-allyl complex (**M2b**), and (iii) methanol and H_2 with the acyl complex (**ML4b**). It is found that methanol coordination to $HCo(CO)_3$, **M2b**,

and **ML4b** is endergonic by 3.7, 29.0, and 12.0 kcal/mol (the corresponding values in solvent are 4.8, 30.8, and 10.4 kcal/mol), respectively. These methanol coordination processes proceed without any additional barriers. The geometry of the transition state **TS(M2b/M2bS)** is similar to that for CO addition (Supporting Information), while no corresponding transition states can be located for the other methanol coordination processes. Comparing these energy data with the free energy barriers of competing reaction steps, we can find that methanol coordination is not favored over butadiene coordination (2.2 kcal/mol) and CO addition (23.5 kcal/mol), while is competitive to H_2 coordination (12.1 kcal/mol) kinetically (the corresponding values in solvent are −1.1, 24.4, and 12.4 kcal/mol, respectively). The thermodynamic properties of these competing reactions are described by the following equations (eqs 3−5).

$$HCo(CO)_3(\eta^2\text{-}H_2C{=}CH{-}CH{=}CH_2)\ (\mathbf{1a}) + CH_3OH = HCo(CO)_3(CH_3OH) + H_2C{=}CH{-}CH{=}CH_2 \quad (3)$$

$$\Delta G[\Delta G_{sol}] = +1.5[+2.4]\ \text{kcal/mol}$$

$$(CH_3{-}CH{=}CH{-}CH_2{-})Co(CO)_4\ (\mathbf{ML3}) + CH_3OH = (CH_3{-}CH{=}CH{-}CH_2{-})Co(CO)_3(CH_3OH) + CO \quad (4)$$

$$\Delta G[\Delta G_{sol}] = +16.3[+19.8]\ \text{kcal/mol}$$

$$(CH_3{-}CH{=}CH{-}CH_2{-}CO{-})Co(CO)_3(\eta^2\text{-}H_2)\ (\mathbf{ML5a}) + CH_3OH = (CH_3{-}CH{=}CH{-}CH_2{-}CO{-})Co(CO)_3(CH_3OH) + H_2 \quad (5)$$

$$\Delta G[\Delta G_{sol}] = -8.3[-3.5]\ \text{kcal/mol}$$

The calculated reaction free energies in eq 3 indicate that the butadiene complex (**1a**) is more stable than the methanol complex by 1.5 kcal/mol in the gas phase or 2.4 kcal/mol in solution. Thus, **1a** is more favored thermodynamically than the methanol complex, and in a possible equilibrium, **1a** should be the major part, while the methanol complex is the minor part. In eq 4, the rather large positive free energies in both the gas phase and solution show that methanol coordination is absolutely not competitive with CO coordination, and therefore, the rate-determining step will not be affected by solvent.

In contrast to butadiene and CO coordination, the negative free energies in eq 5 show that methanol has a large effect on H_2 addition in both the gas phase and solution. This indicates that methanol will hinder the H_2 addition and also the subsequent formation of aldehyde and result in the formation of ester from methanol oxidative addition (hydromethoxycarbonylation). However, it is found that methanol oxidative addition has a much higher activation free energy (ca. 49 kcal/mol[41,42]) than H_2 oxidative addition (ca. 6 kcal/mol, Figure 5), and this indicates that direct methanol oxidative addition is unlikely as compared to H_2 oxidative addition. On this basis, it is easily to explain the accelerating effect of the hydromethoxycarbonylation of 1,3-butadiene by pyridine, since pyridine as base deprotonates methanol to form pyridinium ion and methoxide (CH_3O^-), and CH_3O^- will react with the acyl complex to yield an ester via nucleophilic substitution, as proposed by Tuba et al.[31] This will reduce the rather high methanol oxidative addition barrier.

It is therefore summarized that methanol as solvent can stabilize species of the catalytic cycle, but cannot change the relative free energies on one hand, and on the other hand, methanol as ligand does not compete with CO addition to coordinatively unsaturated species and change the rate-determining step.

Conclusion

At the B3LYP/6-311+G(d) density functional level of theory, the entire catalytic cycle of the $HCo(CO)_3$-catalyzed hydroformylation of butadiene has been investigated. The origin of the observed regioselectivity is clarified. The solvent effects including dielectric effect and the solvation of coordinatively unsaturated species are also elucidated.

Due to the presence of the conjugated structural unit, some crucial reaction behaviors of butadiene hydroformylation strongly differ from those of olefins. The hydroformylation of butadiene can give $H_2C{=}CHCH_2CH_2CHO$ (1,2-addition), $H_3CHC{=}CHCH_2CHO$ (1,4-addition), and $H_2C{=}CHCH(CH_3)CHO$ as initial products. It is found that the *anti*-Markovnikov insertion is reversible, while the Markovnikov insertion is irreversible. The enhanced stability of the *syn*-η^3-allyl complex presents a distinctly thermodynamic preference for the Markovnikov insertion. Therefore, the formation of 1,2-addition product via the *anti*-Markovnikov path is almost suppressed. The CO addition to the *syn*-η^3-allyl complex favors forming the 1,4-addition intermediate over the branched intermediate both kinetically and thermodynamically. Accordingly, the 1,4-addition unsaturated aldehyde $H_3CHC{=}CHCH_2CHO$ should be the principal product, in agreement with the experimental findings. For the most favored path **ML**, the CO addition is the rate-determining step. It is also noted that methanol as solvent and ligand does not change the potential energy surface compared to that found in the gas phase.

Acknowledgment. This work was supported by the Chinese Academy of Sciences (20029908) and the National Natural Science Foundation China.

Supporting Information Available: Total electronic energies, zero-point energies (ZPE), thermal correction to enthalpies, and Gibbs free energies (403.15 K, 200 atm), and the optimized Cartesian coordinates, as well as structures with relative enthalpies for all systems. This material is available free of charge via the Internet at http://pubs.acs.org.

OM0500422

(41) Klaus, S.; Neumann, H.; Jiao, H.; von Wangelin, A. J.; Gördes, D.; Strübing, D. Hübner, S.; Hateley, M.; Weckbecker, K.; Huthmacher, T.; Riermeier, C.; Beller. M. J. *Organomet. Chem.* **2004**, *689*, 3685.

(42) Sweany, R. L. *Organometallics* **1989**, *8*, 175.